Particuology 101 (2025) 155–165

Contents lists available at ScienceDirect

Particuology

journal homepage: www.elsevier.com/locate/partic

# Acoustic emission and machine learning algorithms for particle size analysis in gas-solid fluidized bed reactors

Fria Hossein [a,*], Matteo Errigo [a], Sibo Cheng [b], Massimiliano Materazzi [a], Paola Lettieri [a], Rossella Arcucci [c], Panagiota Angeli [a]

[a] Department of Chemical Engineering, University College London, London, WC1E7JE, UK
[b] CEREA, Ecole des Ponts ParisTech & EdF R&D, Champs-sur-Marne, 77455, France
[c] Department of Earth Science and Engineering, Imperial College London, London, SW7 2AZ, UK

ARTICLE INFO

*Article history:*
Received 30 May 2024
Received in revised form
16 August 2024
Accepted 9 October 2024
Available online 18 October 2024

*Keywords:*
Acoustics
Particle size distribution
Fluidized bed
Inversion
ML
Elastic wave

ABSTRACT

In this work, a combination of an acoustic emission (AE) technique and a machine learning (ML) algorithm (Random Forest (RF) and Gradient Boosting Regressor (GBR)) is developed to characterize the particle size distribution in gas-solid fluidized bed reactors. A theoretical approach to explain the generation of acoustic emission signal in gas-solid flows is presented. An AE signal is generated in gas-solid fluidized beds due to the collision and friction between fluidized particles as well as between particles and the bed inner wall. The generated AE signal is in the form of an elastic wave with frequencies >100 KHz and it propagates through the gas-solid mixture. An inversion algorithm is used to extract the information about the particle size starting from the energy of the AE signal. The advantages of this AE technique are that it is a cheap, sensitive, non-intrusive, radiation-free, suitable for on-line measurements. Combining this AE technique with ML algorithms is beneficial for applications to industrial settings, reducing the cost of signal post-processing. Experiments were conducted in a pseudo-2D flat fluidized bed with four glass bead samples, with sizes ranging from 100 μm to 710 μm. AE signals were recorded with a sampling frequency of 5 MHz. The AE signal post-processing and data preparation for the ML process are explained. For the ML process, the AE frequency, AE energy and particle collision velocity data sets were divided into training (60%), cross-validation (20%) and test sets (20%). Two ensemble ML approaches, namely Random Forest and Gradient Boosting Regressor, are applied to predict particle sizes based on the AE signal features. The combination of these two models results in a coefficient of determination ($R^2$) value greater than 0.9504.



## 1. Introduction

Gas-solid fluidized bed reactors are widely implemented in the pharmaceutical, petrochemical and energy industries (Lettieri & Yates, 2013). Recently, fluidized bed reactors have been increasingly used in applications such as $CO_2$ capture, waste management and hydrogen production, thus contributing to the efforts for net zero (Abanades et al., 2004; Iannello, Morrin, & Materazzi, 2020a, 2020b; Materazzi et al., 2019). The excellent mixing and increased contact between the phases in fluidized-beds allow for enhanced mass and heat transfer rates, making them suitable for challenging reaction systems such as exothermic ones (Kunii & Levenspiel, 1991). Fluidized-bed reactors have long been studied and their overall behaviour is well understood. They are, however, overly complex systems and require constant monitoring during their operation. For instance, the particle size distribution of the bed material may vary throughout operation, due to attrition, in the form of particle fragmentation (Zheng et al., 2020) and surface abrasion (Yang, 2003), as well as because of agglomeration (Bartels et al., 2008; Scala, 2018). The fluidization behaviour and quality are strongly affected by the particle size distribution. Different diagnostic techniques have been applied for the study of such reactors (Grace et al., 2020). However, most of them are not applicable to industrial fluidized-bed reactors due to their size, while some of these techniques are intrusive, or require specific configurations. Pressure measurements can be useful to obtain information about

* Corresponding author.
*E-mail address:* f.hossein@ucl.ac.uk (F. Hossein).

https://doi.org/10.1016/j.partic.2024.10.005

macroscopic properties, as well as changes in the overall bed behaviour (Van ommen & Mudde, 2008); they are widely used due to their simplicity and robustness, but do not provide local information on particle behaviour. X-ray imaging (Lettieri & Yates, 2013), X-ray tomography (Bieberle et al., 2012) and $\gamma$-ray tomography (Van ommen & Mudde, 2008) as well as electrical capacitance tomography (Wang & Yang, 2021), provide detailed information of the inside of gas-solid fluidized-bed reactors, including, among others, voidage distribution and bubble characteristics. Nevertheless, they are hardly used in industrial fluidized-bed systems, as their application entails many safety risks, while the signals are heavily attenuated as they travel through large cross sections. Positron Particle Tracking (PEPT) has been successfully applied in real industrial systems, as noted in the comprehensive guide by (Windows-Yule et al., 2022). Penn et al. (2020) conducted a comprehensive study employing real-time magnetic resonance imaging to examine the flow regimes in a fluidized bed with a gas injection system, identifying six distinct regimes of bubbling and jetting behaviour, proposing an empirical model for predicting jet length based on the Froude number and background gas flow, and analysing the bubble breakoff frequency in the pulsating jet regime using Fourier analysis. Moreover, the post-processing of some of the resulting signals can be quite demanding, thus limiting the online monitoring of the units. Positron emission particle tracking (Windows, Seville, Ingram, & Parker, 2020) and magnetic particle tracking (Sette et al., 2015) enable users to track tracers within fluidized beds, and, indirectly, to obtain a time-averaged particle velocity distribution, but, for statistically valuable information, the measuring times are very long. Magnetic resonance imaging (Penn et al., 2018) allows visualization of 2D slices, returning information on voidage, bubble characteristics and particle velocity distribution. Industrial fluidized-bed reactors, however, are commonly made of stainless-steel walls, which block the radio-frequency signals emitted by the sample. Optical (Sobrino et al., 2009) and capacitance probes (Huang & Lu, 2018) provide local information on properties such as voidage and bubble characteristics, but they are intrusive and can affect the operation of the fluidized system.

There is need for non-intrusive, online, local diagnostic techniques for industrial fluidized-bed reactors that allow monitoring during operation. Acoustic techniques (ultrasound and acoustic emission) are a promising option and a review of their application to particulate flows, including the physical principles, experimental methods, and typical challenges, was given by (Hossein et al., 2021). AE for measuring particle size in solid gas flows offers several advantages, including non-destructive testing, real-time monitoring, and sensitivity to small particles. It is versatile across various materials and requires minimal sample preparation. However, there are challenges, such as complex signal interpretation and sensitivity to environmental noise, which can lead to inaccuracies. AE also requires extensive calibration and specialized knowledge, and high-quality systems can be costly. Ultimately, while AE provides valuable insights, its effectiveness can be limited by the specific application and conditions. In a previous paper (Hossein et al., 2022), we developed ultrasound techniques to characterize the particle size distribution, velocity profiles, and voidage in liquid-solid fluidized beds. Ultrasound sensors, however, operate at high frequency ranges, causing a large attenuation of sound waves, especially in air, since the attenuation is frequency dependent. This makes the use of ultrasound sensors in highly concentrated gas-solid flows difficult. Nevertheless, ultrasound sensors operating at low frequencies (below 500 kHz) have been used to measure low particle volume fractions (<10%) in turbulent granular suspensions in air (Van den Wildenberg et al., 2020).

For gas-particulate systems, AE techniques are more appropriate. In gas-solid fluidized beds, particles collide with each other and with the bed walls. This collision or friction will convert some kinetic energy into elastic waves. The amount of energy converted is dependent on the particle size, on the particle impact velocity with the bed wall or with other particles, as well as on the thermophysical properties of the fluid and of the particles. The generated elastic waves propagate through the fluidized bed and can be detected by an acoustic emission sensor. Different parameters of the recorded acoustic waves such as amplitude, frequency, duration, and energy, can be used to characterize gas-solid fluidized beds. Acoustic emission techniques record the signal generated from a fluidized bed and analyse the relationship between this signal and the fluidized bed properties (Watson et al., 2014). AE techniques have been used to monitor granulation (Hansuld et al., 2012). It has been reported that the frequency of the AE wave is inversely proportional to the particle size (Carson et al., 2008). Boyd and Varley (2001) reviewed the development of AE techniques to monitor physico-chemical changes in chemical engineering processes such as bubble sound in liquid-gas dispersions for characterizing bubble size. Briongos et al. (2006) showed that AE techniques can be used to monitor the slugging behaviour in fluidized beds. Zhang et al. (2019) reported the online measurement of conveyed particles in solid gas flows through AE sensing. They established an AE energy model for plug flow in vertical pneumatic conveying by analysing the acoustic signal of particle-wall interactions. Acoustic emission techniques have previously been applied to fluidized-bed systems to measure the average particle size of the bed material (Zhang et al., 2021). However, in fluidized beds the particles often have a distribution of sizes which, in addition, can significantly change during operation because of phenomena such as comminution and agglomeration. For this reason, evaluating the particle size distribution can be helpful in better understanding and monitoring the operation of a fluidized-bed system.

The main challenge with the use of AE techniques in gas-particle systems is the inversion of the acoustic signal for the calculation of different parameters such as particle size distribution, particle velocity and voidage. Another challenge with acoustic emission techniques is the need of a theoretical model to express the generation of an acoustic emission signal in fluid particle flows.

In this study, we aim to address these challenges. We present a theoretical approach to explain the generation of acoustic emissions signal in gas-solid flows and propose an inversion algorithm to obtain the particle size distribution from the acoustic emission energy spectrum. We apply the methodology to acoustic emission measurements obtained in a pseudo-2D fluidized bed and characterize the particle size distribution for four different particle sample sizes. Furthermore, for the first time, we investigate the application of machine learning (ML) techniques to the inversion of the acoustic emission signal in gas-solid fluidized-bed reactors. Machine learning techniques can alleviate the need for complex signal post processing, reduce the computation time for the inversion while they need fewer signal input parameters. Two ensemble machine learning algorithms, Random Forest (RF) and Gradient Boosting Regressor (GBR), are applied to the acoustic emission signal to predict the particle size distribution based on the frequency, and the kinetic energy of the acoustic emission signal, as well as a particle velocity. These two ML algorithms, based on the decision-tree (DT) framework, have been widely applied in an enormous range of engineering problems (e.g., Bieberle et al., 2012; Cheng et al., 2022; Gong et al., 2023a), thanks to their training efficiency and good interpretability (Salehi-Nik et al., 2009). AE techniques have the potential to deliver accurate information about the bed material as well as the fluid dynamics of a fluidized-bed reactor in a non-invasive way, through opaque systems, and in real time.

In what follows, Section 2 details the acoustic emission theory behind the generation and propagation of an acoustic emission signal in gas-solid flows and introduces the inversion algorithm for obtaining the particle size distribution from the acoustic emission signal energy. Section 3 provides details of the experimental setup, while Section 4 outlines the results and discussion. Section 5 describes the application of machine-learning algorithms on the acoustic emission signal. Finally, section 6 draws some conclusions on the work done.

## 2. Acoustic emission theory and inversion

### 2.1. Theory

Acoustic Emission (AE) in fluid-particle flows refers to the generation of elastic waves by abrupt release of energy (Zhou et al., 2018). The sources of AE signals are particle-particle or particle-wall collisions (impact sound), particle-wall friction (friction sound), and air turbulence (aerodynamic sound) (Salehi-Nik et al., 2009). Since the average time between bursts of emission is usually shorter than the duration of the emission itself, the AE signal may appear as continuous (Addali et al., 2010). To detect these waves, a suitable acoustic emission sensor needs to be mounted on the outer face of the bed wall. The generation of AE waves depends on the colliding particle size, shape, density, and velocity, as well as on the properties of the bed material wall (Wang et al., 2009).

A typical pulse of an AE signal recorded by an acoustic emission sensor in a fluidized bed is shown in Fig. 1. The statistical AE features that can be determined are the peak amplitude of the pulse, the rise-time (time between the initiation of the signal and the peak amplitude), the signal duration (time interval between the start and the end point of the AE signal), the frequency and the absolute energy of the signal. Thanks to this, the AE parameters can be used to obtain the particle size distribution (PSD) in gas-solid flows. To calculate the rise time accurately in the presence of multiple overlapping signals, we implemented advanced signal processing techniques that facilitate the deconvolution of these signals. This approach allows for the isolation of individual contributions, improving the reliability of our rise time measurements, and is complemented by appropriate filtering methods to enhance signal clarity.

The absolute energy $E$ of the AE signal is given by:

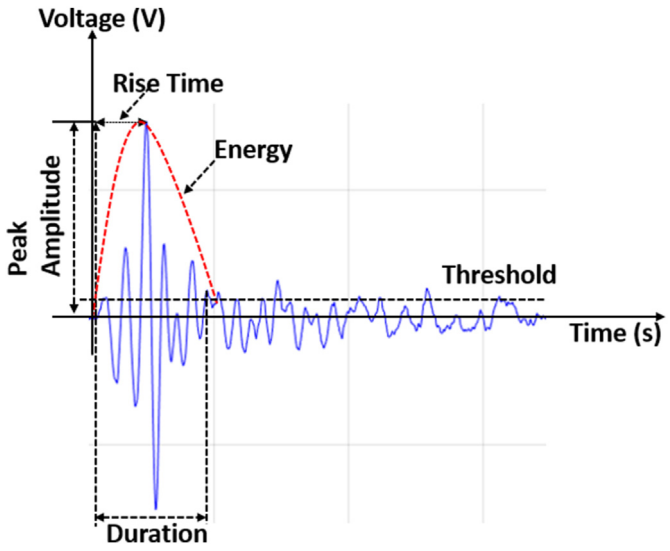


**Fig. 1.** Typical AE pulse signal recorded in a 2D gas-solid fluidized bed.

$$E = \frac{1}{f_s}\sum_{j=1}^{N}\left[A_j\right]^2 \tag{1}$$

where $f_s$ is the sampling frequency, $A_j$ is the signal amplitude of the $j$-th measurement, and $N$ is the number of sampling points of the AE pulse. In the case of a purely elastic collisions between the bed wall and the particles, the energy fraction in the elastic wave $\lambda_e$ (the energy dissipated during the collision process) can be given by (Boettcher et al., 2017):

$$\lambda_e = K\frac{\alpha}{1+e} \tag{2}$$

where $K$ is a proportionality constant and $e$ is the coefficient of restitution, which can be obtained as follows:

$$e = 3.8\sqrt{\left(\frac{\sigma_y}{G}\right)}\left(\frac{2\pi\rho {v_{pi}}^2}{3\sigma_y}\right)^{-\frac{1}{8}} \tag{3}$$

where $\rho$ and $\sigma_y$ are the density and the yield stress of the particle respectively, while $v_{pi}$ is the impact velocity (normal component velocity) of the particle, and $G$ is given by:

$$G = \frac{1-\gamma_1^2}{Y_1} + \frac{1-\gamma_2^2}{Y_2} \tag{4}$$

where $Y_1, Y_2$ and $\gamma_1, \gamma_2$ are the Young's moduli and Poisson's ratios respectively for the particle and the bed wall. Zhang et al. (2021) gave a definition for the dimensionless function $\alpha$ in Eq. (2) as follows:

$$\alpha = \frac{4(1+e)}{F_o^2\omega_p}\int_0^\infty \omega^2|F(\omega)|^2 d\omega \tag{5}$$

where $\omega_p = \left(\frac{3\sigma_y}{2\rho R^2}\right)^{1/2}$, $F_o = \left(\frac{4\pi\rho R^3 v_{pi}\omega_p}{3}\right)$, where $R$ is the particle radius, $F(\omega)$ is the Fourier component of the AE signal in FFT, and $e$ is the coefficient of restitution (Eq. (3)) with values ranging between 0 and 1. The value of 0 corresponds to a perfectly plastic collision and the value of 1 to a perfectly elastic collision. The relationship between $\alpha$ and $1 + e$ is obtained for glass particles (density 2500 kg/m$^3$) with particle size of 100–250 μm and is illustrated in Fig. 2.

The above Eqs. (1)–(5) link the AE energy to the particle size. Function $\alpha$, shown in Fig. 2, depends on the AE energy, the particle size, the mechanical properties of the particle and the coefficient of restitution $e$. To obtain the particle size distribution from the AE energy recorded by the AE sensor, an inversion algorithm is needed, and this is based on the theoretical approach presented so far.

### 2.2. Inversion

The AE signal is generated due to the particle-particle and particle with inner bed wall collisions. The generated AE signals were recorded by an AE sensor (Nano 30, MISTRAS). The AE sensor used here cannot detect signals generated from particle-particle collisions, but it can detect the AE signals generated from the collisions of the particles with the bed wall. Therefore, we are ignoring the AE signals generated due to the particle-particle collisions. Theoretically, the kinetic energy released from the collision of particles with the inner bed wall can be expressed (Whiting et al., 2018) as:

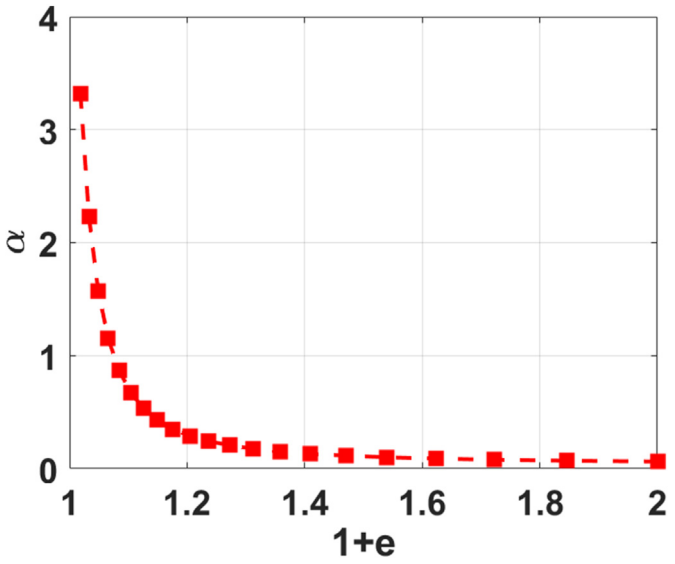


**Fig. 2.** Relationship between the coefficient of restitution $e$, and the dimensionless constant $\alpha$ was calculated with Eq. (3) and Eq. (5) respectively for glass particles (density 2500 kg/m$^3$) with average sample size of 175 μm.

$$E = \lambda_e E_k \tag{6}$$

where $\lambda_e$ is defined by Eq. (2). The kinetic energy $E_k$ is proportional to the diameter and velocity of the impinging particles, and is given by:

$$E_k = \frac{1}{12}\pi\rho d^3 v_{pi}^2 \tag{7}$$

The relationship between the diameter of a particle and AE energy can be obtained by combining Eqs. (2), (6) and (7):

$$d = \left[\frac{12E}{\frac{\alpha}{1+e} K\pi\rho\, v_{pi}^2}\right]^{-\frac{1}{3}} \tag{8}$$

To obtain the particle diameter, the velocity of the impinging particles against the bed wall is required. The component perpendicular to the wall of the particle impact velocity can be related to the gas superficial velocity and the particle diameter by the following equation (Cody et al., 1996):

$$v_{pi} = U\left(\frac{D}{d}\right)\left[1 - \exp\left(-\frac{2\left(U - U_{mf}\right)}{U_{mf}}\right)\right] \tag{9}$$

where $D$ is an empirical constant and can be taken equal to 110 μm for monodispersed glass spheres (Cody et al., 1996), and $d$ is the particle diameter. However, as the particle size follows a distribution, particles move at different velocities. $U$ is the gas superficial velocity (we measured the superficial velocities by increasing the airflow rate using a rotameter and observed the particles beginning to expand within the fluidized reactor), and $U_{mf}$ is the minimum fluidization velocity. This correlation is valid for $1 \leq U/\ U_{mf} \leq 2$. Therefore, the particle size distributions were calculated for all samples with the conditions of $\frac{U}{U_{mf}} = 1.5$. Furthermore, another assumption is that the sensor only records signals when particles collide with the inner bed wall, without capturing any particle-particle collision signals.

After the AE energy $E$ is obtained experimentally, $K$ can be found through experimental calibration as:

$$K = X v_{pi} + X \tag{10}$$

The particle characteristics, and particle size distributions corresponding to each sample are shown in Table 1. The $K$ values obtained from the experiments conducted in a 2D fluidized bed (as depicted in Fig. 4) are pivotal to our analysis. To derive these $K$ values, we initially predicted the values of $v_{pi}$ by utilizing Eq. (9). For each fluidization velocity value $U$, we standardized $U$ to 1.5 times the minimum fluidization velocity, denoted as $U_{mf}$, as per the conditions specified in Eq. (9). The individual $U$ values for each sample were calculated as follows: $U$ (sample 1) = 6.255 cm/s, $U$ (sample 2) = 21.015 cm/s, $U$ (sample 3) = 32.625 cm/s, and $U$ (sample 4) = 45 cm/s.

Subsequently, $K$ values were obtained (using Eq. (10)), for the experiments were conducted in triplicate for every sample to ascertain the $X$ value, resulting in $X$ values of $15 \times 10^{-31}, 14 \times 10^{-31}, 13 \times 10^{-31}$, and $10 \times 10^{-31}$ for samples 1, 2, 3, and 4, respectively. As shown in Fig. 3, the $K$ values for every sample (blue markers) are dependent on particle velocities and it is linearly decreasing for larger samples.

Finally, an inversed Gaussian distribution can be used to fit this particle size data, where the general form of the inversed Gaussian distribution is given by (Murphy, 2007):

$$F(x) = \frac{1}{s\sqrt{2\pi}} \exp\left[-\frac{1}{2}\left(\frac{x - M}{s}\right)^2\right] \tag{11}$$

where, $M$ is the median of variable $x$ and $s$ is the standard deviation of $x$.

In this study, we have assumed a Gaussian distribution to represent the particle size distribution. The Gaussian model is particularly suitable when the particle sizes are symmetrically distributed around a mean value, which aligns with the characteristics of the samples analysed in our experiments. This assumption allows us to simplify the complexity of the particle size distribution while still providing a robust framework for our analysis. Additionally, using a Gaussian distribution facilitates the comparison of our results with previous studies in the literature, where similar assumptions have been effectively employed.

## 3. Experimental setup

Fig. 4 shows the 2D fluidized bed together with the acoustic emission circuit used in this work. The fluidized-bed walls are 10 mm-thick and made of polymethyl methacrylate (PMMA). The fluidized bed height, width and depth are respectively 1000, 100 and 10 mm. Air injection at the bottom of the fluidized bed is controlled by a rotameter, while the distributor is a porous plate with hole size equal to 25 μm. The flow of air, before entering the fluidized bed, is homogenized in a windbox, a plenum filled with ceramic beads approximately 9 mm in diameter.

**Table 1**
Physical properties and minimum fluidization velocities of the particle samples used in the experiments.

| Sample | Size (μm) | Density (kg/m$^3$) | Weight (g) | $U_{mf}$ (cm/s) |
|---|---|---|---|---|
| 1 | 100–250 | 2500 | 350 | 4.17 |
| 2 | 250–355 | 2500 | 350 | 9.34 |
| 3 | 355–500 | 2500 | 350 | 14.5 |
| 4 | 500–710 | 2500 | 350 | 30.0 |

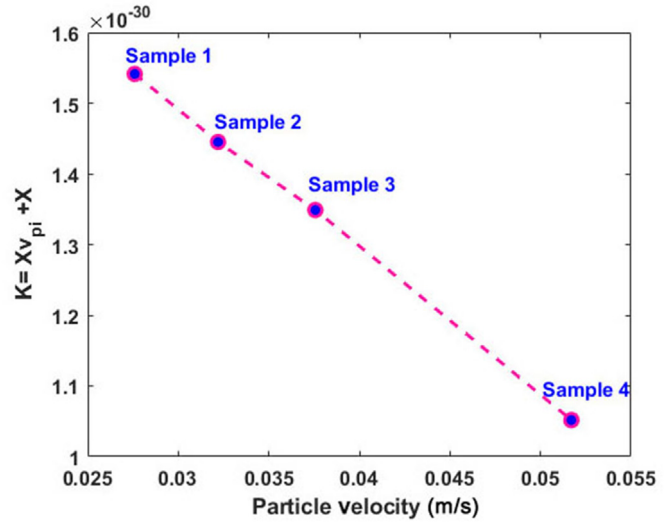


**Fig. 3.** The $K$ values for sample 1, 2, 3 and 4 at $\frac{U}{U_{mf}} = 1.5$ for each sample, and the blue dots represent the $K$ values for each sample, while the pink dashed line illustrates the linear correlation showing how the $K$ value is dependent on $v_{pi}$.

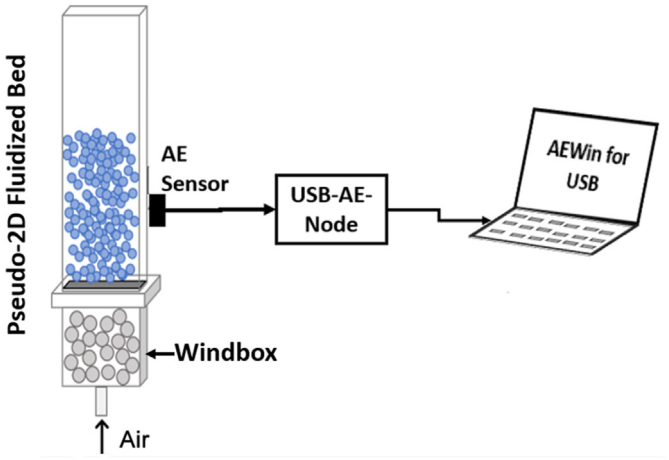


**Fig. 4.** Experimental setup: pseudo-2D flat fluidized bed on the left, acoustic emission sensing circuit on the right.

The particles used in this work are spherical glass beads (ballotini) with density equal to 2500 kg/m$^3$, and the fluidizing gas is air. All experiments were conducted at room temperature and pressure. Four particle samples with varied sizes were used. Their physical properties and minimum fluidization velocities are shown in Table 1.

If the air superficial velocity in the fluidized bed is larger than the minimum fluidization velocity of the sample, particles are fluidized, and collide with the bed walls and with each other. Elastic waves are then generated and recorded by the AE sensor mounted on the outer bed wall, 6 cm above the distributor plate. The particle velocity is calculated from the gas superficial velocity using Eq. (9). The operating specifications of the AE sensor (Nano 30, MISTRAS) are summarised in Table 2. To ensure a good contact between the AE sensor and the bed wall, a vacuum grease is employed. Experiments with the different particle samples were repeated three times each and returned a standard deviation on the AE amplitude of less than 3%.

The AE signal is amplified by up to 45 $dB$ and filtered through a band pass filter with frequency range 0–20 KHz. A signal analyser

**Table 2**
Operating specifications of the AE sensor.

| AE Sensor properties | Values |
|---|---|
| Peak sensitivity | 62 $dB$ |
| Operating frequency range | 125 – 750 KHz |
| Resonant frequency | 300 KHz |
| Temperature range | – 65 – 177 °C |
| Case material | Stainless steel |

(AE-Node, MISTRAS) is used for the wave form acquisition at a sampling rate of 5 MHz. The digitized data is then downloaded onto a computer for further signal post-processing.

The AE signals are recorded for the four different sample sizes (see Table 1), and the energy of the measured AE signal is calculated using Eq. (1). The AE signal is then inverted to particle size distribution using Eq. (8) (see section 2). The equations mentioned here are solved in MATLAB.

## 4. Results and discussion

The AE signal was collected in the experimental setup described above, and the peak amplitude and absolute energy were obtained. As can be seen in Fig. 5, both the average peak amplitude and the absolute energy (from Eq. (1)) increase with particle size and particle impact velocity, and Fig. 5 is showing how AE energy and amplitudes changes with fluidization flow rates. Additionally, the particle impact velocity increases with increasing fluidization velocity, see Eq. (9). This is because the kinetic energy converted into acoustic wave energy is larger for larger or faster particles.

For each sample size (see Table 1), the acoustic emission energy was obtained by using Eq. (1) for fluid flow rates $\frac{U}{U_{mf}} = 1.5$. This was then fed into Eq. (8) to obtain the particle size distribution. The results were also compared with the particle size distributions obtained from images of the samples taken with an Axio Observer 5 (ZEISS) microscope (bars in Fig. 5(b)). The Python cv2.HoughCircles function was used to identify the size of each glass bead in the images (Fig. 5(a)) to obtain the particle size distribution. For each sample size at least 150 beads were measured via imaging to have a statistically valid distribution.

As can be seen from Fig. 5(b) the particle size distributions obtained with the AE technique and from the microscope images are in reasonable agreement. The differences between the two techniques may be attributed to: (1) the large attenuation of the AE signals (signal reflected from the bed wall), which may not reach the sensor; (2) the number of particles imaged with the microscope might not be sufficient; (3) the correlation used to calculate the particle velocity.

The experiments were conducted in a room under controlled temperature and pressure conditions. Hence, the errors due to temperature or pressure changes are considered negligible.

The main challenge remains that the acoustic emission attenuation is not accounted for. The AE signal is generated by the collision or friction of particles with the bed wall and the signal is mainly attenuated due to the reflection of AE signal by the bed wall. The attenuation factor depends on the material properties (e.g., density, compressibility) and frequency of the sound wave ($attenuation \propto \frac{1}{frequency}$). There are other factors causing the attenuation of the sound wave such as absorption, diffraction, divergence, and temperature (Hossein et al., 2021). The attenuation of sound wave through polymethyl methacrylate (PMMA) was measured by (Bloomfield et al., 2000) and it was found equal to 1.4 $dB$/cm/MHz. It is difficult to measure the acoustic emission attenuation in a solid-gas mixture experimentally because the exact location of the

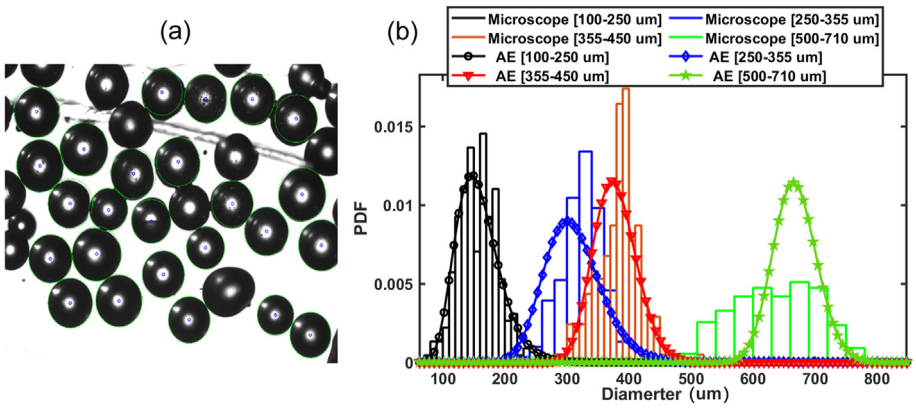


**Fig. 5.** (a) Example of a microscope picture of glass beads, with identified centres (in blue) and circles (in green). A x5 lens was used, with 0.91 μm/pixel conversion. (b) Inverted particle size distribution from the measured AE energy compared to the PSD obtained from the microscope images.

original AE signal is not known. Locating the AE signal would require multiple AE sensors for a small number of AE events. This is particularly challenging in complex flows, where many AE collisions occur at the same time over various locations.

Furthermore, accounting for the acoustic emission attenuation coefficient remains challenging. For this reason, in the next section we are introducing a machine learning algorithm combined with the acoustic emission energy technique presented so far to characterize particle size distributions in gas-solid flows.

To evaluate the accuracy of particle sizes measured by acoustic emission and microscope, the mean square error has been calculated and is presented in Table 3. The results indicate that acoustic emission demonstrates a strong ability to measure particle size distribution with a smaller margin of error compared to the microscope imaging. This suggests that acoustic emission is a reliable technique for accurately assessing particle sizes, providing valuable insights into the particle distribution characteristics.

## 5. Machine learning algorithms coupled with acoustic emission

Recently, ML algorithms have been coupled with acoustic emission techniques (Das et al., 2019). Zhang et al. (2021) introduced a ML framework (based on the frequency of the AE signal) to classify the damage of structural elements. Most recent applications of acoustic emission techniques in combination with machine learning approaches were used for early leak detection in pipelines (Ahn et al., 2019), damage identification (Xu et al., 2019), failure detection in ferro-cement composite structures (Behnia et al., 2016), monitoring gas-liquid mixing in stirred tanks (Forte et al., 2021), and identification of the solid suspension state in a stirred tank (Rossi et al., 2022). Here, we are introducing a methodology to combine the AE technique with ML for predicting the particle size distribution without depending on the model for the particle velocity, which can be difficult to acquire (Hii et al., 2013; Zhang et al., 2019). We built an ML regression model which takes frequency, and kinetic energy from the acoustic signal as inputs and predicts the particle size distribution. In this study, we employ two decision tree (DT)-based ensemble machine learning methods, Random Forest (RF) and Gradient Boosting Regressor (GBR), for predicting particle diameter. RF, utilizing a bagging strategy (which refers to the process of training multiple decision trees on different subsets of the data and then aggregating their predictions to improve accuracy and reduce overfitting) (Gong et al., 2023b; Prasad et al., 2006), trains multiple prediction models in parallel on randomly selected subsets of the training data. It uses Gini coefficients (Lewis, 2000) for tree splitting within the DT framework, offering easier interpretability and less training complexity compared to Neural Network-based algorithms. On the other hand, GBR (Friedman, 2001) builds upon an ensemble of weak learners (DTs), applying a boosting strategy that sequentially trains trees to correct previous errors. This process incrementally builds the model, with each tree focusing on the weaknesses of the combined predictions of the preceding trees. While both methods employ Classification and Regression Trees (CART), the key distinction lies in the RF's simultaneous development of multiple trees in the RF method and in the iterative improvement approach in the GBR method, as detailed in Natekin and Knoll (2013). The methods used in this study can be used for different particle size ranges, and a fair comparison, the hyperparameters of both RF and GBR are fixed as.

- Number of individual models $n_{DT} = 100$,
- Maximum depth of each DT, $d_{DT} = 100$,
- Number of features for each tree split $n_{features} = 3$.

At first, we have evaluated the ML without preprocessing the data as shown in Fig. 6. The raw data included the original signal from the acoustic sensor, signal frequency, and energy. Our ML process involved using Microscope results for label generation, with a 60% training, 20% testing, and 20% validation split. The models, such as random forest and xgboost, were trained using this non-pre-processed data.

Fig. 6 displays the machine learning predictions generated by both the RF and XGBoost models, achieving $R^2$ scores of 0.6480 and 0.5537, respectively. The performance of the predictions with non-pre-processed data is notably poor, primarily attributed to the presence of noise in the data captured by the acoustic emission sensor. This noise can stem from various sources, including background noise. Noise in the experimental data is often non-negligible, because of experimental errors and uncertainty propagations which may result in considerable bias in the predictive model (Gupta & Gupta, 2019). External noise from sources like

**Table 3**
Mean squared values of measured particle sizes from acoustic emission and microscopy.

| Sample | Mean square error |
|---|---|
| 1 | 2.79 |
| 2 | 3.33 |
| 3 | 4.54 |
| 4 | 7.73 |

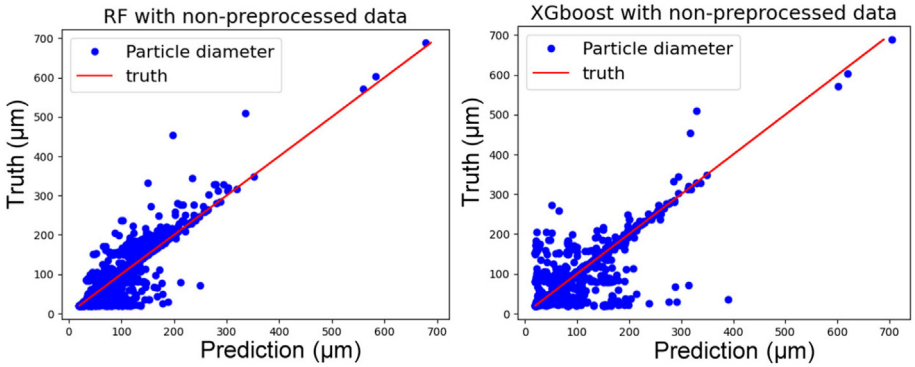


**Fig. 6.** The comparison between predictions and actual values on the non-pre-processed dataset for samples 1, 2, 3, and 4 from Fig. 5(b) is illustrated. The x-axis represents the predicted particle sizes in μm, while the y-axis displays the true values of particle sizes in μm.

combustion and factory operations challenges the effectiveness of our AE technique; however, strategies such as band-pass filtering, advanced machine learning algorithms for noise reduction, strategic sensor placement and directional microphones can improve signal clarity and enhance the signal-to-noise ratio. Continuous monitoring and adaptation of the system can further enhance its robustness against environmental noise, enabling reliable data collection even in challenging industrial settings.

Ensemble ML methods, which consist of a certain number of sub-models, are known to deal efficiently with data uncertainties and imbalance (Verbaeten & Assche, 2003).

To overcome this and improve the prediction results we pre-processed the data for the ML process as: Initially, the acoustic emission signal was cleaned out from all values that are out of the range of the sensor detection (Nano 30, MISTRAS sensor operation frequency range is 125–750 KHz). The AE signal then undergoes Fast Fourier Transform (FFT) to obtain the acoustic signal "fingerprint" in the frequency domain. The amplitudes and frequencies of the signal are then identified. To remove the background noise (defined as a sound within human hearing range, $f <$ 20 KHz), a high-pass filter was applied. Finally, to reduce the data set, which limits the input of the ML process, only frequencies with a high relative variance (from the *FFT* values) are selected. The relative variances ($R_{Fj}$) for each frequency ($j$-th) are calculated as follows (Rossi et al., 2022):

$$R_{Fj} = \frac{\sigma_j^2}{\mu_j} = \frac{\sum_{i=1}^{N} \left(A_{ij} - \mu_j\right)^2}{\sum_{i=1}^{N} A_{ij}} \tag{12}$$

where $N$ is the number of *FFT* spectrum, and $A_{ij}$ is the *FFT* magnitude for the $j$-th frequency (column) for the $i$-th spectrum ($i$-th row), $\mu_j = \frac{1}{M}\sum_{i=1}^{M} A_{ij}$ and $\sigma_j^2 = \frac{1}{M}\sum_{i=1}^{M}(A_{ij} - \mu_j)^2$ .The frequencies with the highest $R_{Fj}$ (relative frequency variances) values and the corresponding AE amplitudes, were selected for each sample. Finally, the training, validation, and test datasets, consisting of 2001 data points from each sample, were used in the ML processing. The data post processing and ML steps are illustrated in Fig. 7.

A detailed illustration of the essential data pre-processing steps necessary for ML data preprocessing is shown in Fig. 8.

In Fig. 8(a), the raw AE signal as captured by the AE sensor is visually presented, providing an initial overview of the data. Transitioning to Fig. 8(b), we delve deeper into the signal processing by highlighting the AE signal in its transformed state through Fast Fourier Transform (FFT), which facilitates the analysis of signal frequencies, Fig. 8(c) offers a closer look at the FFT of the AE signal post-application of a 20 kHz cutoff filter. This filtration step is crucial as it effectively eliminates undesirable background noise, enhancing the quality and reliability of the data under scrutiny. Lastly, Fig. 8(d) shows the frequency reduction process of the AE signal. This reduction is achieved through the implementation of Eq. (12), highlighting a specific computational method used to streamline and refine the signal for subsequent machine learning analysis. Together, these sequential steps depicted in Fig. 8 not only demonstrate the meticulous preparation of the AE data but also underscore the significance of data refinement to optimize the efficiency and accuracy of machine learning algorithms in this work. Finally, Eq. (12) is utilized to determine the relative frequency variances for ML processing. After cleaning and preprocessing the AE data, we have evaluated the ML models again, the raw data included the pre-processed AE signal l frequency, and AE energy. Our ML process involved using microscope image results for label generation, with a 60% training, 20% testing, and 20% validation split, and the results are shown in Fig. 9.

Results in Fig. 9 is showing that, the combination of detailed preprocessing steps and the robust algorithmic frameworks of the machine learning models contribute to their accuracy in predicting particle sizes. The $R^2$ scores on the test dataset for random forest (0.9504) and xgboost (0.9404) further support the efficacy of our approach.

We evaluated the performance of RF and GBR on the test dataset by comparing the model output against the particle diameter measured by the AE technique, as shown in Fig. 9. For both approaches the predicted value is remarkably close to the recorded experimental results of the test set (the test particle sizes measured by the AE technique, see Fig. 6(b)) data was used as a label.

Table 4 presents compelling evidence of the robust performance of the regression models with pre-processed data, as indicated by $R^2$ values exceeding 0.9 for both approaches. These outcomes align consistently with the observations depicted in Fig. 9. Notably, the RF model slightly outperforms the GBR model based on both metrics. Additionally, Fig. 10 delves into the feature importance of the predictive models, employing permutation importance to assess the significance of each input variable, as proposed by Altmann et al., in 2010.

Fig. 10 illustrates the feature importance analysis for the machine learning predictions, revealing the dominance of AE energy over AE frequency in influencing the model's predictions. Furthermore, the visualization in Fig. 10 highlights the importance of extracted AE features, such as AE frequency and AE energy, derived from the pre-processed data in influencing the machine learning

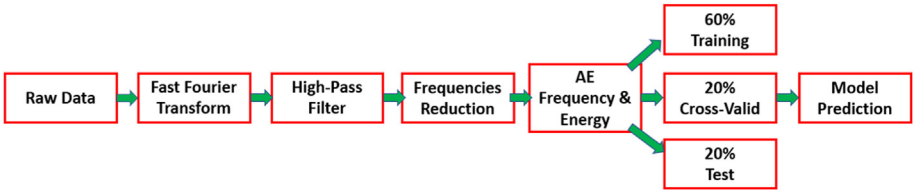


**Fig. 7.** Data preparation and processing for ML.

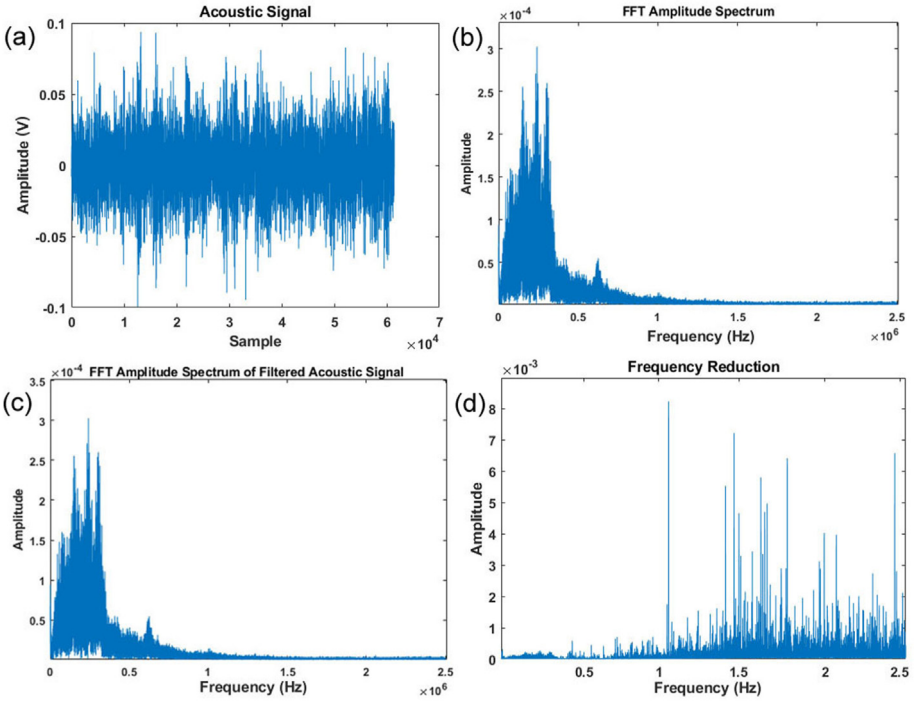


**Fig. 8.** The frequency reduction process for ML.

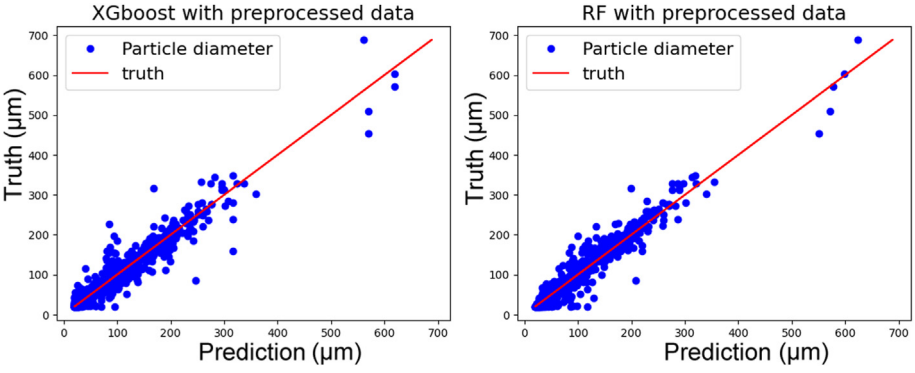


**Fig. 9.** The comparison between predictions and actual values on the pre-processed dataset for samples 1, 2, 3, and 4 from Fig. 5(b) is illustrated. The x-axis represents the predicted particle sizes in μm, while the y-axis displays the true values of particle sizes in μm. The validation process encompasses the entire dataset, including all samples.

**Table 4**
The $R^2$ evaluated on the test set with preprocessed and non-preprocessed data.

| ML Algorithm | Non-preprocessed $R^2$ | Preprocessed $R^2$ |
|---|---|---|
| RF | 0.6480 | 0.9504 |
| GBR | 0.5537 | 0.9404 |

model predictions, and this is in line with the recent work in the literature reported by (Hii et al., 2013; Zhang et al., 2019).

A notable revelation from Fig. 10 is the prominence of Kinetic Energy over particle frequency when the model is trained on pre-processed data, a coherence with Eq. (10) where AE energy is contingent on particle sizes. This relationship stems from the fact that collisions involving larger particles generate higher AE energy,

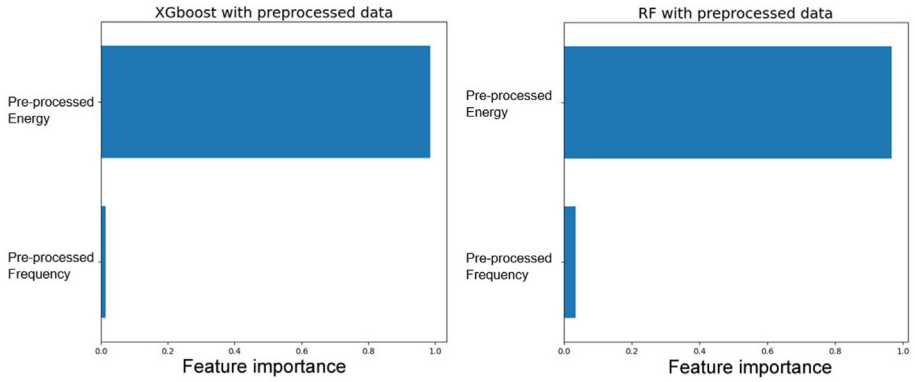


**Fig. 10.** Feature importance (with permutation) in RF and GBR models with pre-processed data.

while smaller particles produce relatively lower energy at the same velocities.

It is also discerned that the importance attributed to AE frequency is notably less in comparison to kinetic energy. This discrepancy could be attributed to potential limitations of the sensor in recording AE signal frequencies, constrained within the range of 125 – 750 KHz, shaping the observed patterns in the feature importance analysis.

The machine learning methods implemented in this study do not only provide an accurate prediction of the particle size distribution, but also bring more insight in understanding the relationship between particle size, kinetic energy, and AE frequency. The test and training data can be accessed via https://github.com/DL-WG/Acoustic_emission_-_ML.

The transferability of this method to different system materials, particle types, and varying operational conditions, such as temperature, gas density, and viscosity, is an important consideration. While the principles of measuring particle size distribution using AE are broadly applicable, the model may require retraining to account for changes in system dynamics and particle properties. Complete retraining may not always be necessary; fine-tuning or transfer learning techniques could be employed instead. Training and calibration in an industrial setting can be feasible with proper integration of the sensor system and data collection protocols, allowing for effective adaptation to various operational environments.

Our method can be adapted for binary, ternary, or polydisperse systems with varying particle densities by modifying the machine learning model to include features related to density and mass in addition to size. This involves enhancing the feature extraction and expanding the calibration process to accommodate diverse particle compositions, ultimately improving the model's predictive accuracy. Additionally, integrating various sensors or measurement techniques may be necessary to capture interactions among particles with different densities and sizes, ensuring reliable predictions of particle size distribution in complex systems.

These factors highlight the need for careful consideration of the specific application when deploying the method in real-world scenarios.

## 6. Conclusions

This study presents the combination of acoustic emission and machine learning approaches for obtaining particle size distribution in fluidized-bed reactors. Each particle colliding against the fluidized-bed inner wall releases energy in the form of an elastic wave. This phenomenon is called acoustic emission and can be used to draw information about the collision itself. The acoustic emission particle size distributions were compared against imaging results of the bed material. Once the technique has been calibrated, the recorded acoustic emission signal can be used to obtain the current particle size distribution within the fluidized-bed reactor. This could be very useful in applications where the size distribution of the bed particles varies in time. In the second part of the study, acoustic emission was combined with machine learning to improve the accuracy of the inversion algorithm. In the machine learning process, we utilized the inputs of energy, frequency, and collision velocity directly to predict the particle size distributions. However, the theoretical model is presented to provide mathematical descriptions or representations of the physical phenomena and underlying principles associated with acoustic emission. By implementing ensemble learning methods, an accurate prediction of the particle size can be achieved. The developed regression functions could help in improving the results of the acoustic emission technique. The data processing in this study was conducted offline; however, we can adapt the method for online processing in future implementations. In conclusion, the combination of acoustic emission and machine learning seems promising in delivering a cheap and non-invasive tool for real-time measurements of the particle size distribution in a fluidized-bed reactor and enable optimization of its operation.

## CRediT authorship contribution statement

**Fria Hossein:** Writing – review & editing, Writing – original draft, Validation, Methodology, Formal analysis, Data curation, Conceptualization. **Matteo Errigo:** Writing – review & editing, Methodology. **Sibo Cheng:** performed the ML part, writing and data processing. **Massimiliano Materazzi:** Writing – review & editing. **Paola Lettieri:** Writing – review & editing, Supervision. **Rossella Arcucci:** Writing – review & editing, Supervision. **Panagiota Angeli:** Writing – review & editing, Supervision.

## Declaration of competing interest

The authors declare that they have no known competing financial interests or personal relationships that could have appeared to influence the work reported in this paper.

## Acknowledgments

The authors would like to acknowledge the support from Engineering and Physical Sciences Research Council, UK, through the PREMIERE Programme Grant (EP/T000414/1). M Errigo would also like to thank the Department of Chemical Engineering, UCL for his studentship.

## References

Abanades, J. C., Aanthony, E. J., Lu, D. Y., Salvador, C., & Alvarez, D. (2004). Capture of $CO_2$ from combustion gases in a fluidized bed of CaO. *AIChE Journal, 50*, 1614–1622.

Addali, A., Al-Lababidi, S., Yeung, H., Mba, D., & Khan, F. (2010). Acoustic emission and gas-phase measurements in two-phase flow. *Proceedings of the Institution of Mechanical Engineers - Part E: Journal of Process Mechanical Engineering, 224*, 281–290.

Ahn, B., Kim, J., & Choi, B. (2019). Artificial intelligence-based machine learning considering flow and temperature of the pipeline for leak early detection using acoustic emission. *Engineering Fracture Mechanics, 210*, 381–392.

Altmann, A., Toloşi, L., Sander, O., & Lengauer, T. (2010). Permutation importance: A corrected feature importance measure. *Bioinformatics, 26*(10), 1340–1347.

Bartels, M., Lin, W., Nijenhuis, J., Kapteijn, F., & Van Omen, J. R. (2008). Agglomeration in fluidized beds at high temperatures: Mechanisms, detection, and prevention. *Progress in Energy and Combustion Science, 34*, 633–666.

Behnia, A., Ranjbar, N., Chai, H. K., & Masaeli, M. (2016). Failure prediction and reliability analysis of ferrocement composite structures by incorporating machine learning into acoustic emission monitoring technique. *Construction and Building Materials, 122*, 823–832.

Bieberle, M., Barthel, F., & Hampel, U. (2012). Ultrafast X-ray computed tomography for the analysis of gas–solid fluidized beds. *Chemical Engineering Journal, 189*, 356–363.

Bloomfield, P. E., Wei-Jung, L., & Lewin, P. A. (2000). Experimental study of the acoustical properties of polymers utilized to construct PVDF ultrasonic transducers and the acousto-electric properties of PVDF and P(VDF/TrFE) films. *IEEE Transactions on Ultrasonics, Ferroelectrics, and Frequency Control, 47*, 1397–1405.

Boettcher, R., Kunik, M., Eichmann, S., Russell, A., & Mueller, P. (2017). Revisiting energy dissipation due to elastic waves at impact of spheres on large thick plates. *International Journal of Impact Engineering, 104*, 45–54.

Boyd, J. W., & Varley, J. (2001). The uses of passive measurement of acoustic emissions from chemical engineering processes. *Chemical Engineering Science, 56*, 1749–1767.

Briongos, J. V., Aragón, J. M., & Palancar, M. C. (2006). Fluidised bed dynamics diagnosis from measurements of low-frequency out-bed passive acoustic emissions. *Powder Technology, 162*, 145–156.

Carson, G., Mulholland, A. J., Nordon, A., Tramontana, M., Gachagan, A., & Hayward, G. (2008). Particle sizing using passive ultrasonic measurement of particle–wall impact vibrations. *Journal of Sound and Vibration, 317*, 142–157.

Cheng, S., Jin, Y., Harrison, S. P., Quilodrán-Casas, C., Prentice, I. C., Guo, Y.-K., & Arcucci, R. (2022). Parameter flexible wildfire prediction using machine learning techniques: Forward and inverse modelling. *Remote Sensing, 14*, 3228.

Cody, G. D., Goldfarb, D. J., Storch, G. V., & Norris, A. N. (1996). Particle granular temperature in gas fluidized beds. *Powder Technology, 87*, 211–232.

Das, A. K., Suthar, D., & Leung, C. K. (2019). Machine learning based crack mode classification from unlabeled acoustic emission waveform features. *Cement and Concrete Research, 121*, 42–57.

Forte, G., Alberini, F., Simmons, M., & Stitt, H. E. (2021). Use of acoustic emission in combination with machine learning: Monitoring of gas–liquid mixing in stirred tanks. *Journal of Intelligent Manufacturing, 32*, 633–647.

Friedman, J. H. (2001). Greedy function approximation: A gradient boosting machine. *Annals of Statistics, 29*, 1189–1232.

Gong, H., Tao, Z., Zhang, C., Wan, Y., & Li, Q. (2023a). Parameter identification and state estimation for nuclear reactor operation digital twin. *Annals of Nuclear Energy, 180*(2023), Article 109497.

Gong, H., Tao, Z., Zhang, C., Wan, Y., & Li, Q. (2023b). Parameter identification and state estimation for nuclear reactor operation digital twin. *Annals of Nuclear Energy, 180*, Article 109497.

Grace, J. R., Bi, X., & Ellis, N. (2020). *Essentials of fluidization technology*. John Wiley & Sons.

Gupta, S., & Gupta, A. (2019). Dealing with noise problem in machine learning datasets: A systematic review. *Procedia Computer Science, 161*, 466–474.

Hansuld, E. M., Briens, L., Sayani, A., & McCann, J. A. B. (2012). Monitoring quality attributes for high-shear wet granulation with audible acoustic emissions. *Powder Technology, 215–216*, 117–123.

Hii, N. C., Tan, C. K., Wilcox, S. J., & Chong, Z. S. (2013). An investigation of the generation of acoustic emission from the flow of particulate solids in pipelines. *Powder Technology, 243*, 120–129.

Hosseini, F., Materazzi, M., Errigo, M., Angeli, P., & Lettieri, P. (2022). Application of ultrasound techniques in solid-liquid fluidized bed. *Measurement: Journal of the International Measurement Confederation, 194*.

Hosseini, F., Materazzi, M., Lettieri, P., & Angeli, P. (2021). Application of acoustic techniques to fluid-particle systems: A review. *Chemical Engineering Research and Design, 176*, 180–193.

Huang, J., & Lu, Y. (2018). Characteristics of bubble, cloud, and wake in jetting fluidized bed determined using a capacitance probe. *Chemical Engineering Research and Design, 136*, 687–697.

Iannello, S., Morrin, S., & Materazzi, M. (2020a). Fluidised bed reactors for the thermochemical conversion of biomass and waste. *KONA Powder and Particle Journal, 37*, 114–131.

Iannello, S., Morrin, S., & Materazzi, M. (2020b). Fluidized bed reactors for the thermochemical conversion of biomass and waste. *KONA Powder and Particle Journal, 37*, 114–131.

Kunni,D. & Levenspiel, O. (213). Fluidization enginzering Elsevier.

Lettieri, P., & Yates, J. G. (2013). *New generation X-ray imaging for multiphase systems*.

Lewis, R. J. (2000). An introduction to classification and regression tree (CART) analysis. *Annual meeting of the society for academic emergency medicine*. Citeseer.

Materazzi, M., Taylor, R., & Cairns-Terry, M. (2019). Production of biohydrogen from gasification of waste fuels: Pilot plant results and deployment prospects. *Waste Management, 94*, 95–106.

Murphy, K. P. (2007). Conjugate Bayesian analysis of the Gaussian distribution. *Defense, 1*, 16.

Natekin, A., & Knoll, A. (2013). Gradient boosting machines: A tutorial. *Frontiers in Neurorobotics, 7*, 21.

Penn, A., Boyce, C. M., Kovar, T., Tsuji, T., Pruessmann, K. P., & Müller, C. R. (2018). Real-time magnetic resonance imaging of bubble behavior and particle velocity in fluidized beds. *Industrial & Engineering Chemistry Research, 57*, 9674–9682.

Penn, A., Boyce, C. M., Prussmann, K. P., & Muller, C. R. (2020). Regimes of jetting and bubbling in a fluidized bed studied using real-time magnetic resonance imaging. *Chemical Engineering Journal, 383*, Article 123185.

Prasad, A. M., Iverson, L. R., & Liaw, A. (2006). Newer classification and regression tree techniques: Bagging and random forests for ecological prediction. *Ecosystems, 9*, 181–199.

Rossi, A., Alberini, F., & Brunazzi, E. (2022). Identification of suspension state using passive acoustic emission and machine learning in a solid–liquid mixing system. *Chemical Engineering Research and Design, 177*, 273–282.

Salehi-Nik, N., Sotudeh-Gharebagh, R., Mostoufi, N., Zarghami, R., & Mahjoob, M. J. (2009). Determination of hydrodynamic behavior of gas–solid fluidized beds using statistical analysis of acoustic emissions. *International Journal of Multiphase Flow*.

Scala, F. (2018). Particle agglomeration during fluidized bed combustion: Mechanisms, early detection, and possible countermeasures. *Fuel Processing Technology, 171*, 31–38.

Sette, E., Pallares, D., Johnsson, F., Ahrentorp, F., Ericsson, A., & Johansson, C. (2015). Magnetic tracer-particle tracking in a fluid dynamically down-scaled bubbling fluidized bed. *Fuel Processing Technology, 138*, 368–377.

Sobrino, C., Acosta-Iborra, A., Santana, D., & De Vega, M. (2009). Bubble characteristics in a bubbling fluidized bed with a rotating distributor. *International Journal of Multiphase Flow, 35*, 970–976.

Van Den Wildenberg, S., Jia, X., & Roche, O. (2020). Acoustic probing of the particle concentration in turbulent granular suspensions in air. *Scientific Reports, 10*, Article 16544.

Van ommen, J. R., & Mudde, R. F. (2008). Measuring the gas-solids distribution in fluidized beds–A review. *International Journal of Chemical Reactor Engineering, 6*.

Verbaeten, S., & Assche, A. V. (2003). Ensemble methods for noise elimination in classification problems. *International workshop on multiple classifier systems* (pp. 317–325). Springer.

Wang, J., Rrn, C., Yang, Y., & Hou, L. (2009). Characterization of particle fluidization pattern in a gas solid fluidized bed based on acoustic emission (AE) measurement. *Industrial & Engineering Chemistry Research, 48*, 8508–8514.

Wang, H., & Yang, W. (2021). Application of electrical capacitance tomography in pharmaceutical fluidised beds–a review. *Chemical Engineering Science, 231*, Article 116236.

Watson, N., Povey, M., Reynolds, G., Xu, B., & Ding, Y. (2014). Acoustic emission monitoring from a lab scale high shear granulator—a novel approach. *International Journal of Pharmaceutics, 465*, 262–274.

Whiting, J., Springer, A., & Sciammarella, F. (2018). Real-time acoustic emission monitoring of powder mass flow rate for directed energy deposition. *Additive Manufacturing, 23*, 312–318.

Windows, C., Seville, J., Ingram, A., & Parker, D. (2020). Positron emission particle tracking of granular flows. *Annual Review of Chemical and Biomolecular Engineering, 11*, 367–396.

Windows-Yule, K., Nicusan, L., Herald, M. T., Manger, S., & Parker, D. (2022). *Positron emission particle tracking: A comprehensive guide*. IOP Publishing.

Xu, D., Liu, P., Li, J., & Chen, Z. (2019). Damage mode identification of adhesive composite joints under hygrothermal environment using acoustic emission and machine learning. *Composite Structures, 211*, 351–363.

Yang, W. C. (2003). Handbook of fluidization and fluid-particle systems. *China Particuology, 1*, 137.

Zhang, G., Yan, Y., Hu, Y., & Zheng, G. (2019). On-line size measurement of pneumatically conveyed particles through acoustic emission sensing. *Powder Technology, 353*, 195–201.

Zhang, G., Yan, Y., Hu, Y., & Zheng, G. (2021). Investigations into the sensing mechanism of acoustic emission sensors for particle size measurement in a particular case: Normal incidence. *Measurement Science and Technology, 32*, Article 075107.

Zheng, D., Huang, T. H., Yan, J., Yang, H., Peng, C., Fu, Y., & Li, B. (2020). Coupling of abrasion attrition theory with mechanical characteristics for particle attrition in a fluidized bed reactor. *Asia-Pacific Journal of Chemical Engineering, 15*, Article e2544.

Zhou, Y., Yang, L., Lu, Y., Hu, X., Luo, X., & Chen, H. (2018). Flow regime identification in gas-solid two-phase fluidization via acoustic emission technique. *Chemical Engineering Journal, 334*, 1484–1492.